Conservation of angular momentum in ultrafast spin dynamics

Jacopo Simoni[1,*] and Stefano Sanvito[2]

[1]*Molecular Foundry, Lawrence Berkeley National Laboratory, Berkeley, California 94720, USA*
[2]*School of Physics and CRANN institute, Trinity College, Dublin 2, Ireland*

The total angular momentum of a closed system is a conserved quantity, which should remain constant in time for any excitation experiment once the pumping signal has been extinguished. Such conservation, however, is never satisfied in practice in any real-time first-principles description of the demagnetization process. Furthermore, there is growing experimental evidence that the same takes place in experiments. The missing angular momentum is usually associated to lattice vibrations, which are not measured experimentally and are never considered in real-time simulations. Here we critically analyze the issue and conclude that current state-of-the-art simulations violate angular momentum conservation already at the electronic level of description. This shortcoming originates from an oversimplified description of the spin-orbit coupling, which includes atomic contributions but neglects completely that of itinerant electrons. We corroborate our findings with time-dependent simulations using model tight-binding Hamiltonians, and show that indeed such conservation can be reintroduced by an appropriate choice of spin-orbit coupling. The consequences of our findings on recent experiments are also discussed.

I. INTRODUCTION

Thanks to recent advances in femtosecond laser technologies the possibility of achieving control over the magnetization dynamics at timescales of the order of 100 fs is now within our reach. After the discovery of the ultrafast optical demagnetization of a nickel film irradiated with a subpicosecond laser pulse in 1996 [1], several additional experiments have shown a rich variety of laser-induced phenomena in magnetic compounds, including ultrafast demagnetization [2–8], spin reorientation [9,10], and the modifications of the magnetic structure [11,12].

Such race toward the control of the magnetization dynamics at the femtosecond timescale is driven by both the fundamental physical investigation of the underlying mechanism leading to ultrafast spin dynamics and technological innovation in the fields of high-speed magnetic recording and spin electronics [13–15].

The now-standard pump-probe experimental protocol represents a valid technique for probing the magnetization dynamics of a sample at short timescales. Here, the system is first excited by the application of an optical pulse (pump), and then the magnetization dynamics is reconstructed by probing it with a second small perturbing signal (probe) [16,17]. Depending on the time delay between the pump and the probe one can accurately trace the magnetization trajectory with a few femtoseconds' resolution. Then, the results are typically rationalized by choosing among the most relevant dissipation mechanisms that are at play at the given timescale. In partic-

ular, the different types of magnetization dynamics have been usually classified within two main groups.

Fast magnetization processes [18] are those observed on a timescale ranging from a few nanoseconds to a hundred picoseconds. These are usually described by means of the so-called three-temperature model, where electrons, phonons, and spins form three different thermal baths that are brought out of equilibrium by the application of the laser pulse. The subsystems are able to exchange energy and they thermalize to achieve a final equilibrium state.

An *ultrafast* process, instead, is active at a much shorter timescale, approximately of the order of 100 fs. In this case there is much less general agreement on the ultimate cause behind the observed spin dynamics. In recent years different magnetization dynamics models have been proposed in the literature to account for the experimental observations. These include the fully relativistic direct transfer of angular momentum from the laser field to the spins [19,20]; electron-magnon spin-flip scattering [21], where the main channel of spin dissipation is associated to the scattering between conduction electrons and localized magnetic moments; electron-electron spin-flip scattering [22]; the Elliott-Yafet mechanism [23]; other spin relaxation channels due to elastic deformations [24]; and laser-induced superdiffusive spin currents [25]. Among these different schemes only the last one does not require the spin-orbit coupling to play a dominant role in the demagnetization process. Crucially, it was experimentally observed that during the ultrafast demagnetization the behavior of the electronic orbital momentum alone cannot account for the spin decay rate in magnets [26]. Thus, several theoretical works [27,28] suggested that at least part of the spin momentum should be directly transferred to the atomic degrees of freedom. However, the question has not been settled yet, and

___
*jsimoni@lbl.gov

there is still some debate on the importance of such angular-momentum transfer channel and its relation to the ultrafast demagnetization process.

In our contribution we analyze these issues in great detail, in particular focusing on the conservation of the total electronic angular momentum. We find that the standard treatment of the spin-orbit interaction, based on the sum of atomic contributions, is at the origin of the violation of the electronic angular momentum conservation. Relaxing some of the approximations, and in particular the assumption that in a multiatom environment the spin-orbit interaction could still be written as if the atoms were isolated, leads to a more complete expression for the spin-orbit interaction. This allows one to satisfy the conservation law. Our results are put to the test with a simple tight-binding model and confirmed by time-dependent simulations.

In Sec. II we will discuss the problem of the total orbital momentum conservation, in particular, with reference to the *ab initio* methods that are more commonly used to simulate these processes. In Sec. III we explain why these methods cannot conserve the total system's angular momentum at the present level of development and show how to modify the spin-orbit coupling operator in order to enforce this conservation law. In Sec. IV we look at some results obtained in the case of a very simple tight-binding model simulation for atomic clusters and we compare the results with the ones obtained by using the standard models. In Sec. V we conclude.

II. NONCONSERVATION OF THE TOTAL ANGULAR MOMENTUM IN *AB INITIO* SPIN DYNAMICS

The general assumption underpinning any state-of-the-art work in the field of ultrafast magnetism is that the total angular momentum of the system, $\hat{\mathbf{J}}$, is conserved during the dynamics. This means that the following equation holds in general [29]:

$$\Delta \langle \hat{\mathbf{J}} \rangle = \Delta \langle \hat{\mathbf{S}} \rangle + \Delta \langle \hat{\mathbf{L}}^{\mathrm{e}} \rangle + \Delta \langle \hat{\mathbf{L}}^{\mathrm{atom}} \rangle + \Delta \langle \hat{\mathbf{L}}^{\mathrm{ph}} \rangle = 0, \quad (1)$$

where $\hat{\mathbf{S}}$ is the spin operator, $\hat{\mathbf{L}}^{\mathrm{e}}$ the electronic orbital momentum operator, $\hat{\mathbf{L}}^{\mathrm{atom}}$ the atomic orbital momentum, and $\hat{\mathbf{L}}^{\mathrm{ph}}$ the orbital momentum carried by the electromagnetic field interacting with the material. In Eq. (1) the symbol $\langle \hat{\mathbf{O}} \rangle = \langle \hat{\mathbf{O}} \rangle_t$ represents the expectation value of the vector operator $\hat{\mathbf{O}}$ at time t. Under this assumption the nuclear spin degrees of freedom are not considered, since they do not contribute appreciably to the spin dynamics. In fact, the typical energy scale of hyperfine interactions is in the MHz range; namely it is orders of magnitude smaller than the other interactions at play. As such, it starts to influence the magnetization dynamics on a timescale of a few μs, much longer than the temporal scale we are interested in here.

Different models tend to simplify Eq. (1) by assuming that only a few of those terms are involved in the dynamics. For instance in Ref. [20] the spin-relaxation rate is quantified by considering only the transfer between $\hat{\mathbf{S}}$ and the photon field $\hat{\mathbf{L}}^{\mathrm{ph}}$, while Ref. [24] and Ref. [23] consider the spin relaxation due to respectively the phonon field and the full atomic field $\hat{\mathbf{L}}^{\mathrm{atom}}$. In spin-magnon scattering models the spin operator is partitioned into a localized magnetic moment component and an electronic spin one [21]. In Ref. [28] the rate of exchange

of orbital momentum between spin, electrons, and phonons is treated instead at the perturbative level.

When simulating the magnetization dynamics in real time, none of the methods routinely used to interpret the experiments is able to satisfy Eq. (1). These include *ab initio* approaches, such as real-time time-dependent density functional theory (rtTDDFT) [30,31], semi-*ab-initio* schemes, such as time-dependent tight-binding (TDTB) models [32], or quantum chemistry methods [33]. In general, this deficiency is not due to a lack of numerical accuracy; instead it represents a well-known limitation of the underpinning theoretical formalism. The most promising among these methods, both in terms of lack of free parameters and ease of computation, is certainly rtTDDFT [34]. In rtTDDFT only the electronic subsystem is evolved quantum mechanically by solving a set of single-particle Schrödinger-like equations, known as the Kohn-Sham equations [35]. By solving exactly the rtTDDFT problem, it is possible to reproduce the temporal dependence of both the electronic and the magnetization density. However, the interactions between the electrons, the atoms, and the laser field are treated by means of effective external scalar potentials. This means that, in practice, the photons and the atomic degrees of freedom are not self-consistently evolved during the dynamics. As a consequence, only $\Delta \langle \hat{\mathbf{S}} \rangle + \Delta \langle \hat{\mathbf{L}}^{\mathrm{e-KS}} \rangle$ is accessible from the knowledge of the spin and charge densities, where $\hat{\mathbf{L}}^{\mathrm{e-KS}}$ is the electron KS angular momentum [36]. Unfortunately, as one can deduce from Eq. (1), $\Delta \langle \hat{\mathbf{S}} \rangle + \Delta \langle \hat{\mathbf{L}}^{\mathrm{e-KS}} \rangle$ is not a constant of motion. Hence, if we insist on this level of description, we will not be able to answer the question on what is the relevant channel for angular momentum dissipation during the demagnetization process. The same considerations are of course valid also for TDTB models, which are based on a similar approach.

In the remaining part of this section we will look at how $\Delta \langle \hat{\mathbf{S}} \rangle$ and $\Delta \langle \hat{\mathbf{L}}^{\mathrm{e}} \rangle$ evolve in time by solving the set of rtTDDFT equations at the level of implementation provided by the OCTOPUS code [37]. OCTOPUS expands the wave function and the operators in real space over a numerical grid and approximates the electron-ion interaction with norm-conserving pseudopotentials [38] incorporating relativistic effects through a spin-orbit coupling term [39]. In particular, the pseudopotential, $\hat{V}_{\mathrm{ps}}(r)$, has the following general form [40],

$$\hat{V}_{\mathrm{ps}}(r) = \sum_{l} \sum_{m=-l}^{l} V_l^{\mathrm{ps}}(r) \, |l, m\rangle \, \langle l, m| ,$$

$$V_l^{\mathrm{ps}}(r) = \bar{V}_l^{\mathrm{ion}}(r) + \frac{V_l^{\mathrm{SO}}(r)}{4} + \lambda V_l^{\mathrm{SO}}(r) \hat{\mathbf{L}}_0 \cdot \hat{\mathbf{S}}, \quad (2)$$

where $\hat{\mathbf{L}}_0$ is the orbital momentum operator of the atom and the expansion is performed over its eigenstates $|l, m\rangle$ (spherical harmonics). In Eq. (2) the scalar component of the potential, $\bar{V}_l^{\mathrm{ion}}(r)$, describes the effect of the mass shift and the Darwin term, while $V_l^{\mathrm{SO}}(r)$ sets the range of the spin-orbit coupling that, for convenience, we can rescale by a factor λ. We start by considering the simplest possible case of an iron atom isolated in vacuum and excited by the application of an external laser pulse. This example, of course, has little practical relevance, but it has important implications
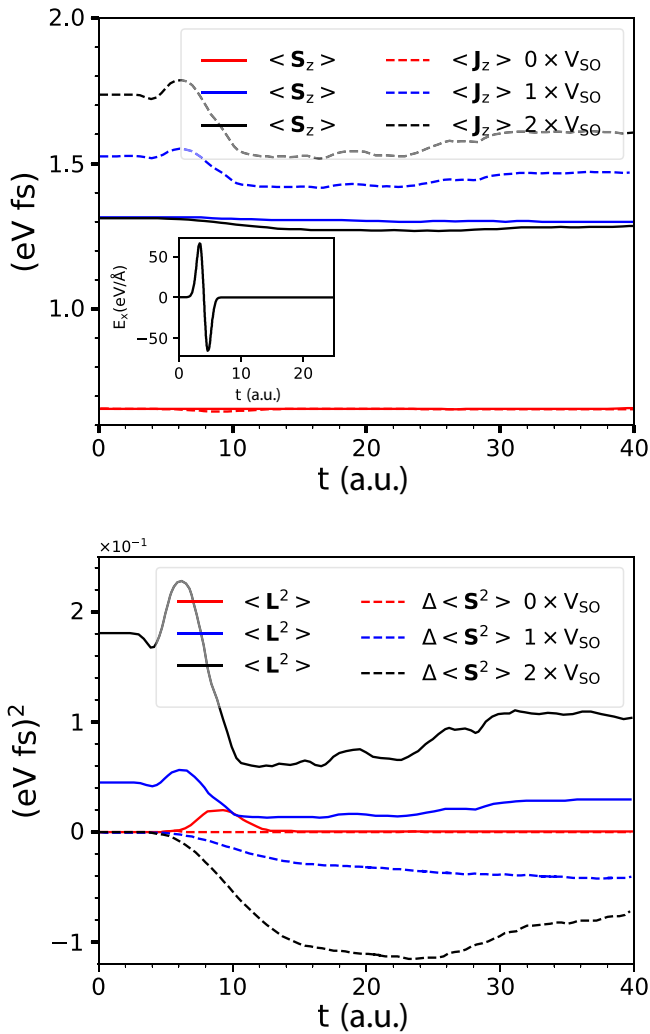
FIG. 1. Time evolution of different observables, as computed with rtTDDFT, for an isolated Fe atom excited by the application of an external laser field, $E_x(t)$, along the x axis (solid black line, upper panel inset). The comparison between $\langle \hat{S}_z \rangle$ (solid line) and $\langle \hat{J}_z \rangle$ (dashed line) is shown in the upper panel for different spin-orbit coupling strengths λV_l^{SO} ($\lambda = 0, 1, 2$). In the lower panel, instead, we show $\langle \hat{\mathbf{L}}^2 \rangle$ (solid line) and $\Delta \langle \hat{\mathbf{S}}^2 \rangle$ (dashed line) obtained with the same values of λ shown in the upper panel. The units for $\langle \hat{S}_z \rangle$ and $\langle \hat{J}_z \rangle$ are eV fs, while that for the electric field is eV/Å.
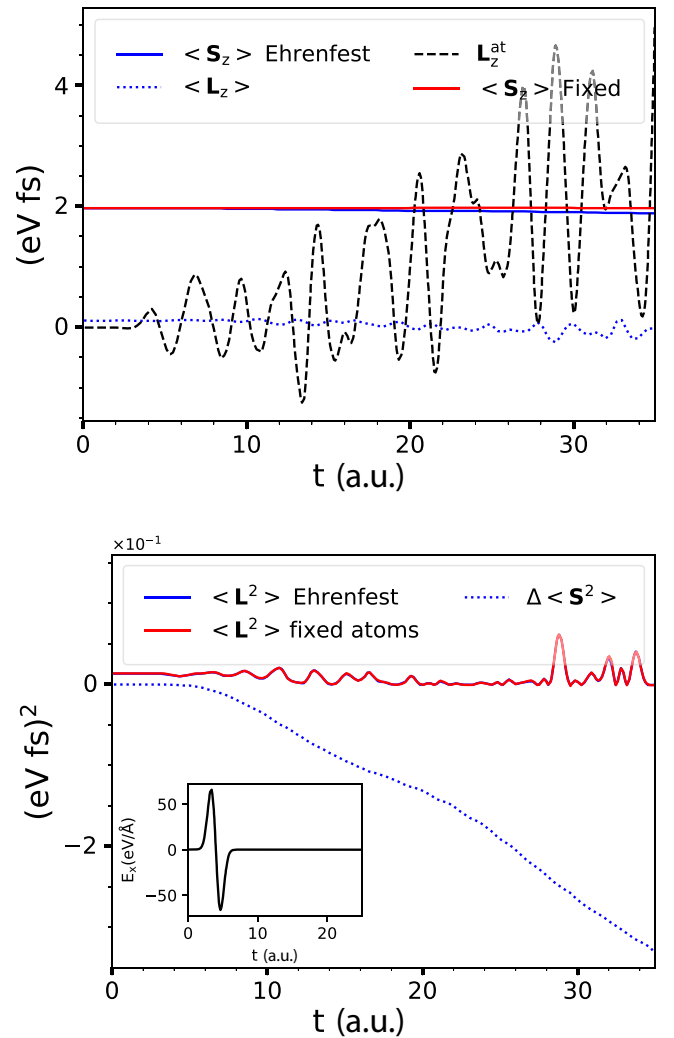

FIG. 2. Time evolution, as computed with rtTDDFT, of different observables for an iron dimer excited by the application of an external laser field, $E_x(t)$, along the x axis (bond axis, solid black line, lower panel inset) in the presence of spin-orbit coupling. The comparison between $\langle \hat{S}_z \rangle$ (solid line) and $\langle \hat{L}_z^e \rangle$ (dotted line) is shown in the upper panel. It is obtained by fixing the atomic positions during the dynamics and by performing a Ehrenfest molecular dynamics calculations. In this last case also the total atomic orbital momentum is shown (dashed black line). In the lower panel we show instead $\langle \hat{\mathbf{L}}_e^2 \rangle$ (solid line) and $\Delta \langle \hat{\mathbf{S}}^2 \rangle$ (dotted line) obtained for *fixed atoms* and for Ehrenfest dynamics calculations. The units for $\langle \hat{S}_z \rangle$ and $\langle \hat{J}_z \rangle$ are eV fs, while that for the field is eV/Å.

for our analysis. In the case of a single isolated atom, the $\langle \hat{\mathbf{L}}^{atom} \rangle$ term is identically zero, so that, after the electric field has extinguished, the quantity $\langle \hat{\mathbf{J}} \rangle = \langle \hat{\mathbf{S}} \rangle + \langle \hat{\mathbf{L}}^e \rangle$ is conserved. This, however, is not the case, as one can see from the time-dependent traces of Fig. 1. We find, in fact, that the total orbital momentum $\langle \hat{J}_z \rangle$ still oscillates even after the laser pulse has vanished. Importantly, we notice a difference between the calculations performed with and without spin-orbit coupling. If the spin-orbit strength, λ, is set to zero (red lines) $\langle \hat{S}_z \rangle$ does not change in time, whereas $\langle \hat{J}_z \rangle$ is affected only during the application of the pulse. For $\lambda = 1, 2$, instead, $\langle \hat{J}_z \rangle$ is not conserved even after the application of the pulse with the fluctuations getting larger as the spin-orbit strength increases. The lower panel of Fig. 1 confirms these findings by showing that $\langle \hat{\mathbf{L}}_e^2 \rangle$ remains constant over long times only in the ab-

sence of spin-orbit coupling. In contrast, for $\lambda \neq 0$ the module squared of the orbital momentum is not conserved during the evolution, even at times where the laser pulse is not present.

The next level of complexity is achieved by looking at a Fe_2 ferromagnetic dimer. In this case we first obtain the electronic ground state at the optimized geometry and then we let the system evolve in time under the effect of the same laser field of Fig. 1, polarized along the bond axis of the dimer. In the simulation the atomic degrees of freedom are explicitly included by performing the rtTDDFT evolution together with Ehrenfest molecular dynamics for the ions [41]. In Fig. 2 we compare the temporal evolution obtained without allowing the atomic

motion to that obtained from Ehrenfest dynamics. In the upper panel we look at $\langle \hat{L}_z^e \rangle$ and $\langle \hat{S}_z \rangle$ and we note that the atomic motion plays no role in their dynamics (the curves obtained with Ehrenfest dynamics overlap perfectly with the ones obtained by keeping the atoms fixed except for $\langle \hat{S}_z \rangle$ where the two curves slightly diverge at longer times). The timescale is, in fact, too short and the atoms do not have enough time to move. In the case of fixed atomic coordinates the quantity $\langle \hat{L}_z^e \rangle + \langle \hat{S}_z \rangle$ is not conserved, as expected. However, also the quantity $\langle \hat{L}_z^e \rangle + \langle \hat{S}_z \rangle + L_z^{\text{atom}}$ is not conserved during the Ehrenfest dynamics. In particular, the atomic orbital momentum is characterized by huge oscillations persisting also after the pulse amplitude sets to zero. In the lower panel of Fig. 2 it is confirmed that the spin lost during the dynamics is not transferred to the orbital degrees of freedom. The same conclusions are valid for both atomic clusters and bulk systems, and increasing the size of the cluster does not help to reinstate angular momentum conservation (see also Ref. [31]).

In the next section we will critically review the approximations taken in our time-dependent simulations and show that the explicit form of spin-orbit potential used is the source of the nonconservation of the angular momentum. Such oversimplified description of the spin-orbit coupling can be corrected and the conservation reinstated.

III. BREAKDOWN OF THE CONSERVATION LAW AND SOLUTION

For the remaining of the paper we will focus on finite-size systems; however, these arguments can be generalized also to the case of extended, periodic systems.

A. Case 1: $\hat{H}_{\text{SO}} = 0$

The first case we analyze corresponds to the situation where there is no spin-orbit interaction. As a consequence, our attention is focused on the conservation of the total angular momentum only (we do not consider the spin; given that it commutes with the system's Hamiltonian, it is a constant of motion). We start by writing the Hamiltonian $\hat{H}$ of a system of N_e electrons in the field generated by N_i identical ions of mass M (we make this choice to keep the treatment easier). Here the ions are treated also as quantum particles; there is no additional external field. The Hamiltonian thus writes

$$\hat{H} = \sum_{a=1}^{N_i} \frac{\hat{\mathbf{P}}_a^2}{2M} + \hat{V}_{\text{ii}} + \hat{H}_{\text{ie}}(\hat{\mathbf{r}}, \hat{\mathbf{p}}, \hat{\mathbf{R}}), \quad (3)$$

where $(\hat{\mathbf{r}}, \hat{\mathbf{p}})$ defines the set of electronic positions and linear momentum operators, $\hat{\mathbf{R}} = (\hat{R}_{1,x}, \hat{R}_{1,y}, \dots, \hat{R}_{N_i,z})$ is the set of $3N_i$ atomic coordinate operators, $\hat{V}_{\text{ii}}$ is the ion-ion interaction, and $\hat{H}_{\text{ie}}$ represents the full electronic Hamiltonian. This latter includes the electron kinetic energy term, the electron-electron interaction, and the electron-ion interaction. By using $d\hat{\mathbf{R}}_a/dt = \hat{\mathbf{P}}_a/M$, it is easy to show that the time derivative of the orbital momentum associated to ion a is

$$\frac{d}{dt}\hat{\mathbf{L}}_a = -\hat{\mathbf{R}}_a \times \nabla_{\mathbf{R}_a}[\hat{H}_{\text{ie}} + \hat{V}_{\text{ii}}]; \quad (4)$$

by writing $\hat{H}_{\text{ie}} = \hat{H}_{\text{ie}}^0 + \hat{U}_{\text{ee}}$, where $\hat{U}_{\text{ee}}$ is the electron-electron interaction potential and $\hat{H}_{\text{ie}}^0 = \sum_{i=1}^{N_e} \hat{\mathbf{p}}_i^2/2m_e +$

$\sum_{i=1}^{N_e} \sum_{a=1}^{N_i} v_{\text{ie}}(|\hat{\mathbf{r}}_i - \hat{\mathbf{R}}_a|)$, with $v_{\text{ie}}(|\hat{\mathbf{r}}_i - \hat{\mathbf{R}}_a|)$ being the electrostatic potential exerted by the ath ion on the ith electron, it is easy to show that

$$\frac{d}{dt}\hat{\mathbf{L}}_a = -\hat{\mathbf{R}}_a \times \left[\sum_{i=1}^{N_e} \nabla_{\mathbf{R}_a} v_{\text{ie}}(|\hat{\mathbf{r}}_i - \hat{\mathbf{R}}_a|) + \nabla_{\mathbf{R}_a} \hat{V}_{\text{ii}} \right]$$

$$= -\sum_{i=1}^{N_e} \hat{\mathbf{r}}_i \times \nabla_{\mathbf{R}_a} v_{\text{ie}}(|\hat{\mathbf{r}}_i - \hat{\mathbf{R}}_a|) - \hat{\mathbf{R}}_a \times \nabla_{\mathbf{R}_a} \hat{V}_{\text{ii}}; \quad (5)$$

by combining Eq. (5) with the time derivative of the ionic linear momentum operator, $d\hat{\mathbf{P}}_a/dt = -\nabla_{\mathbf{R}_a}[\hat{H}_{\text{ie}} + \hat{V}_{\text{ii}}]$, we obtain the following important relation,

$$\frac{d}{dt}\hat{\boldsymbol{\mathcal{L}}}_a = \frac{d}{dt}\left\{ \hat{\mathbf{L}}_a - \sum_{i=1}^{N_e} \hat{\mathbf{r}}_i \times \hat{\mathbf{P}}_a \right\}$$

$$= -\frac{1}{m_e} \sum_{i=1}^{N_e} \hat{\mathbf{p}}_i \times \hat{\mathbf{P}}_a + \sum_{i=1}^{N_e} \hat{\mathbf{r}}_i \times \nabla_{\mathbf{R}_a} \hat{V}_{\text{ii}} - \hat{\mathbf{R}}_a \times \nabla_{\mathbf{R}_a} \hat{V}_{\text{ii}}, \quad (6)$$

from which we can conclude that $\sum_{a=1}^{N_i} \hat{\boldsymbol{\mathcal{L}}}_a$ is a constant of motion for the system's Hamiltonian $\hat{H}$,

$$\frac{d}{dt}\sum_{a=1}^{N_i} \hat{\boldsymbol{\mathcal{L}}}_a = 0 \quad (7)$$

(further details are given in Appendix A). From now on we will refer to $\hat{\boldsymbol{\mathcal{L}}}_a$ as the *conserved orbital momentum* (COM) operator. In addition, we can write $\sum_{a=1}^{N_i} \hat{\boldsymbol{\mathcal{L}}}_a = \hat{\mathbf{L}}^{\text{atom}} + \hat{\mathbf{L}}^e$ with Eq. (1) being manifestly satisfied in the case of a spin-unpolarized system with no externally applied electromagnetic field. It may be also useful to separate the electronic contribution to the COM from the ionic one; by defining $\hat{\boldsymbol{\mathcal{L}}}_a^e = -\sum_{i=1}^{N_e} \hat{\mathbf{r}}_i \times \hat{\mathbf{P}}_a$ we can finally write $\hat{\boldsymbol{\mathcal{L}}}_a = \hat{\mathbf{L}}_a + \hat{\boldsymbol{\mathcal{L}}}_a^e$.

1. Proof of the inequality $\hat{\boldsymbol{\mathcal{L}}}_a^e \neq \hat{\mathbf{L}}_a^0$

Let us define the angular momentum $\hat{\mathbf{L}}_a^0$ as that associated to the atom a in the absence of other nuclei; this operator commutes with the Hamiltonian of the isolated atom: $\hat{H}_{\text{ie}}^a = \sum_{i=1}^{N_e} \hat{\mathbf{p}}_i^2/2m_e + \sum_{i=1}^{N_e} v_{\text{ie}}(|\hat{\mathbf{r}}_i - \hat{\mathbf{R}}_a|) + \hat{U}_{\text{ee}}$. In general it is easy to show that for every multiatom system the inequality $[\sum_{a=1}^{N_i} \hat{\mathbf{L}}_a^0, \hat{H}_{\text{ie}}] \neq 0$ is valid due to the broken spherical symmetry of the system [namely to the term $\sum_{i=1}^{N_e} \sum_{b \neq a}^{N_i} v_{\text{ie}}(|\hat{\mathbf{r}}_i - \hat{\mathbf{R}}_b|)$].

From the previous considerations we have also $[\sum_{a=1}^{N_i} \hat{\boldsymbol{\mathcal{L}}}_a, \hat{H}_{\text{ie}} + \hat{V}_{\text{ii}}] = 0$, while for the purely electronic part of the COM we write $-i[\hat{\boldsymbol{\mathcal{L}}}_a^e, \hat{H}_{\text{ie}}]/\hbar = \hat{\mathbf{R}}_a \times \nabla_{\mathbf{R}_a} \hat{H}_{\text{ie}}$. In general it can be shown that $-i[\hat{\mathbf{L}}_a^0, \hat{H}_{\text{ie}}]/\hbar \neq \hat{\mathbf{R}}_a \times \nabla_{\mathbf{R}_a} \hat{H}_{\text{ie}}$ (all the details are given in Appendix B) and, as a consequence, $\hat{\boldsymbol{\mathcal{L}}}_a^e \neq \hat{\mathbf{L}}_a^0$. In conclusion the electronic orbital momentum operator corresponding to $\hat{\mathbf{L}}^e = \sum_{a=1}^{N_i} \hat{\boldsymbol{\mathcal{L}}}_a^e$ cannot be identified with the sum of the operators $\hat{\mathbf{L}}_a^0$ for isolated atoms.

2. Isolated-atom case

In the case of a single isolated atom we have $[\hat{\mathbf{L}}_a^0, \hat{H}_{ie}^a] = 0$ due to spherical symmetry, in addition $\nabla_{\mathbf{R}_a} \hat{H}_a^a = 0$, and, as a consequence, $\hat{\boldsymbol{\mathcal{L}}}_a^e = \hat{\mathbf{L}}_a^0 + \mathbf{c}\hat{\mathbb{I}}$, where we can freely set $\mathbf{c} = 0$.

3. Nonconservation of $\hat{\mathbf{L}}_{at} + \hat{\mathbf{L}}_{elec}$ in TDTB

In TDTB models the electronic orbital momentum operator around each atom is usually set by definition to $\hat{\boldsymbol{\mathcal{L}}}_a^e = \hat{\mathbf{L}}_a^0$. The time derivative of the expectation value of the electronic orbital momentum operator around atom a is (see Appendix B)

$$
\frac{d}{dt}\mathbf{L}_a^0 = -\frac{i}{\hbar}\langle[\hat{\mathbf{L}}_a^0, \hat{H}_{ie} + \hat{V}_{ii}]\rangle = -\frac{i}{\hbar}\langle[\hat{\mathbf{L}}_a^0, \hat{H}_{ie}]\rangle
$$

$$
\neq \mathbf{R}_a \times \langle\nabla_{\mathbf{R}_a}\hat{H}_{ie}\rangle + \mathbf{R}_a \times \nabla_{\mathbf{R}_a}V_{ii} = -\frac{d}{dt}\mathbf{L}_a^{atom}, \quad (8)
$$

which leads to

$$
\frac{d}{dt}\sum_{a=1}^{N_i}\mathbf{L}_a^0 + \frac{d}{dt}\mathbf{L}^{atom} \neq 0. \quad (9)
$$

As a consequence these models cannot conserve the total orbital momentum even if the atoms are allowed to move. Note that this result is independent on the choice of $\hat{H}_{ie}$ while $\hat{U}_{ee}$ is usually parametrized by means of a mean-field approximation [32].

B. Case 2: $\hat{H}_{SO} \neq 0$

Here we consider the case of finite spin-orbit coupling, so that the spin degrees of freedom need to be reintroduced in the discussion. We will not generalize the treatment to the full Dirac formalism, since it is unnecessary for our conclusions, and so we will simply add the spin-orbit coupling term to the general Hamiltonian of Eq. (3). The spin-orbit coupling operator associated to atom a may be written in the following general form,

$$
\hat{H}_a^{SO} = -\frac{e\hbar}{4m_e^2c^2}\sum_{i=1}^{N_e}\hat{\boldsymbol{\sigma}}_i \cdot [\tilde{\mathbf{E}}_a(\hat{\mathbf{r}}_i, t) \times \hat{\mathbf{p}}_i], \quad (10)
$$

where $\tilde{\mathbf{E}}_a(\hat{\mathbf{r}}, t)$ is the effective screened electric field due to atom a and experienced by the electrons. From now on we will treat the electron-electron interaction in a mean-field way, so that the expression for the effective field can be written as $\tilde{\mathbf{E}}_a(\hat{\mathbf{r}}, t) = \mathbf{E}_{ext}(t)/N_i + \tilde{\mathbf{E}}_a^{mf}(\hat{\mathbf{r}} - \hat{\mathbf{R}}_a)$, where $\tilde{\mathbf{E}}_a^{mf}$ is short range due to the screening of the conduction electrons, while $\mathbf{E}_{ext}$ is the applied external field assumed to be spatially homogeneous. In this way the electrons are treated as effective noninteracting particles. By summing over all the atoms the spin-orbit Hamiltonian becomes

$$
\hat{H}^{SO} = \hat{H}^{SO-ext} + \sum_{a=1}^{N_i}\hat{H}_a^{SO}, \quad \text{where} \quad (11)
$$

$$
\hat{H}^{SO-ext} = -\frac{e\hbar}{4m_e^2c^2}\left[\mathbf{E}_{ext}(t) \cdot \sum_{i=1}^{N_e}\hat{\mathbf{p}}_i \times \hat{\boldsymbol{\sigma}}_i\right],
$$

$$
\hat{H}_a^{SO} = -\frac{e\hbar}{4m_e^2c^2}\sum_{i=1}^{N_e}\hat{\boldsymbol{\sigma}}_i \cdot [\tilde{\mathbf{E}}_a^{mf}(\hat{\mathbf{r}}_i - \hat{\mathbf{R}}_a) \times \hat{\mathbf{p}}_i]. \quad (12)
$$

The first contribution due to the externally applied electric field is not of great interest here since it will act only during the application of the laser pulse, while we are mainly interested in the long-term dynamics of the system; therefore, we will focus on the second term only. Without any loss of generality we can rewrite the mean-field screened electric field as $e\tilde{\mathbf{E}}_a^{mf} = -\nabla_{\mathbf{R}_a}\tilde{v}_{ie}(|\mathbf{r} - \mathbf{R}_a|)$, where $\tilde{v}_{ie}$ is the screened electron-ion potential. The spin-orbit coupling operator then becomes

$$
\hat{H}_{SO}^a = \frac{i}{2m_e^2c^2\hbar}\sum_{i=1}^{N_e}\hat{\mathbf{S}}_i \cdot \{[\hat{\mathbf{P}}_a, \tilde{v}_{ie}(|\hat{\mathbf{r}}_i - \hat{\mathbf{R}}_a|)] \times \hat{\mathbf{p}}_i\}
$$

$$
= \frac{1}{2m_e^2c^2}\sum_{i=1}^{N_e}\sum_{ljk}\epsilon_{ljk}\hat{S}_i^l\hat{P}_a^j\left\{-\frac{i}{\hbar}[\hat{p}_i^k, \tilde{v}_{ie}(|\mathbf{r} - \mathbf{R}_a|)]\right\}
$$

$$
+ \frac{i}{2m_e^2c^2\hbar}\sum_{i=1}^{N_e}\sum_{ljk}\epsilon_{ljk}\hat{S}_i^l[\hat{P}_a^j\hat{p}_i^k, \tilde{v}_{ie}(|\hat{\mathbf{r}}_i - \hat{\mathbf{R}}_a|)]. \quad (13)
$$

After some manipulations the second term on the right-hand side can be shown to be exactly zero. Thus, the spin-orbit coupling experienced by a single electron becomes

$$
\hat{H}_{SO}^a = -\frac{\partial_r\tilde{v}_{ie}(r)}{2m_e^2c^2|\hat{\mathbf{r}} - \hat{\mathbf{R}}_a|}\hat{\mathbf{S}} \cdot \{(\hat{\mathbf{R}}_a - \hat{\mathbf{r}}) \times \hat{\mathbf{P}}_a\}
$$

$$
= -\frac{\partial_r\tilde{v}_{ie}(r)}{2m_e^2c^2|\hat{\mathbf{r}} - \hat{\mathbf{R}}_a|}\hat{\mathbf{S}} \cdot \hat{\boldsymbol{\mathcal{L}}}_a, \quad (14)
$$

where $\hat{\boldsymbol{\mathcal{L}}}_a$ is the COM operator introduced in Eq. (6). It is evident that $\sum_{a=1}^{N_i}\hat{\boldsymbol{\mathcal{L}}}_a$ is not a constant of motion of the new Hamiltonian $\hat{H}' = \hat{H} + \hat{H}_{SO}$, with $\hat{H}$ given by Eq. (3). In particular from Eq. (14), by writing $\hat{H}_{SO} = \sum_a f_a(\mathbf{r})\hat{\boldsymbol{\mathcal{L}}}_a \cdot \hat{\mathbf{S}}$, it is easy to show that

$$
[\hat{\boldsymbol{\mathcal{L}}}_a, \hat{H}_{SO}] = (\hat{\mathbf{R}}_a - \hat{\mathbf{r}}) \times \sum_{b=1}^{N_i}[\hat{\mathbf{P}}_a, f_b(\hat{\mathbf{r}})]\hat{\boldsymbol{\mathcal{L}}}_b \cdot \hat{\mathbf{S}}
$$

$$
+ \sum_{b=1}^{N_i}f_b(\hat{\mathbf{r}})[\hat{\boldsymbol{\mathcal{L}}}_a, \hat{\boldsymbol{\mathcal{L}}}_b] \cdot \hat{\mathbf{S}}, \quad (15)
$$

where the first term on the right-hand side is exactly zero. Furthermore, given the fact that $\hat{\boldsymbol{\mathcal{L}}}_a$ is a generator of the spatial rotation group and satisfies the commutation relations $[\hat{\mathcal{L}}_{a,x}, \hat{\mathcal{L}}_{b,y}] = i\hbar\delta_{a,b}\sum_z\varepsilon_{xyz}\hat{\mathcal{L}}_{a,z}$, we easily obtain $d\hat{\boldsymbol{\mathcal{L}}}_a/dt = f_a(\mathbf{r})\hat{\mathbf{S}} \times \hat{\boldsymbol{\mathcal{L}}}_a$. Since $d\hat{\mathbf{S}}/dt = \sum_{a=1}^{N_i}f_a(\mathbf{r})\hat{\boldsymbol{\mathcal{L}}}_a \times \hat{\mathbf{S}}$ we conclude that $d\hat{\mathbf{J}}/dt = 0$ with $\hat{\mathbf{J}} = \sum_{a=1}^{N_i}\hat{\boldsymbol{\mathcal{L}}}_a + \hat{\mathbf{S}}$.

Nonconservation of the orbital momentum in noncollinear TDDFT

The nonconservation of the total angular momentum in the rtTDDFT simulations presented in Figs. 1 and 2 and reported previously in Ref. [31] is due to the fact that the system's spin-orbit coupling operator (introduced via the pseudopotential approximation) is given by $\hat{H}_{SO}(\mathbf{r}) = \sum_{a=1}^{N_i}\hat{V}_{ps}^{SO}(\mathbf{r} - \mathbf{R}_a)$ and it is a function of the isolated atom orbital momentum operator $\hat{\mathbf{L}}_0$. As a consequence $d\hat{\boldsymbol{\mathcal{L}}}_a/dt \neq f_a(\mathbf{r})\hat{\mathbf{S}} \times \hat{\boldsymbol{\mathcal{L}}}_a$ and $\hat{\mathbf{J}}$ is not a constant of motion. Note that also $\sum_{a=1}^{N_i}\hat{\mathbf{L}}_a^0 + \hat{\mathbf{S}}$ is not

a constant of motion, since $\sum_{a=1}^{N_i} \hat{\mathbf{L}}_a^0$ does not commute with the crystal field Hamiltonian $\hat{H}_{\text{ie}}^0$.

IV. RESULTS

In this section we consider a set of different atomic clusters and we analyze their temporal evolution by using the correct orbital-momentum-conserving spin-orbit coupling [see Eq. (14)]. The results are then compared with the approximated, non-orbital-momentum-conserving evolution. For the analysis we use a TB approximation, whose Hamiltonian writes as follows:

$$\hat{H}(t) = \sum_{a=1}^{N_i} \frac{\mathbf{P}_a^2}{2M} + \hat{H}_{\text{ie}}^{[\mathbf{R}]}(t) + V_{\text{ii}}(\mathbf{R}) + \sum_{a=1}^{N_i} Z_a^* e \mathbf{R}_a \cdot \mathbf{E}(t),$$
(16)

$$\hat{\tilde{H}}_{\text{ie}}^{[\mathbf{R}]}(t) = \sum_{a=1}^{N_i} \sum_i \epsilon_{ai} \hat{c}_{ai}^\dagger \hat{c}_{ai} - \sum_{a<b} \sum_{i<j} \left[t_{ab}^{ij}(\mathbf{R}) \hat{c}_{bj}^\dagger \hat{c}_{ai} + \text{H.c.} \right]$$
$$+ \hat{H}_{\text{SO}}^{[\mathbf{R}]} + \hat{\mathbf{D}} \cdot \mathbf{E}(t).$$
(17)

In the electronic Hamiltonian, $\hat{H}_{\text{ie}}^{[\mathbf{R}]}$, the first two terms on the right-hand side correspond to $\hat{H}_{\text{ie}}^0$, namely to the electron-ion interaction and the electronic kinetic energy (this term can also eventually include a mean-field expression for the electron-electron interaction, not considered here). The last term on the right-hand side is the electric dipole interaction ($\hat{\mathbf{D}} = -e\hat{\mathbf{r}}$). We have further defined Z_a^* as the effective atomic number and $\mathbf{E}(t)$ as the externally applied electric field.

A. Comparison between the two types of evolution

Here we compare the temporal evolution of an atomic dimer under the effect of the two different spin-orbit coupling operators introduced in the previous section. The basis set is built of the s and p orbitals of the two atoms. The model here for explanatory reasons does not have to be physically realistic and we will focus on more realistic systems in future works. In addition the model depends on a set of free parameters that are set arbitrarily and varied in order to look at their influence on the dynamics. These are hopping terms t_{ss}, t_{sp}, and t_{pp}, the spin-orbit strengths λ_a, the on-site energies ϵ_{ai}, and the electric dipole parameters. The atoms are assumed from now on to be identical. The two spin-orbit operators considered here are

$$\hat{H}_{\text{SO}}^0 = \sum_{a=1}^{N_i} \lambda_a \hat{\mathbf{L}}_a^0 \cdot \hat{\mathbf{S}},$$
(18)

$$\hat{H}_{\text{SO}} = \sum_{a=1}^{N_i} \lambda_a \hat{\boldsymbol{\mathcal{L}}}_a \cdot \hat{\mathbf{S}},$$
(19)

where $\hat{\boldsymbol{\mathcal{L}}}_a$ is the previously defined COM operator

$$\hat{\boldsymbol{\mathcal{L}}}_a = \hat{\mathbf{L}}_a - \sum_{i=1}^{N_e} \hat{\mathbf{r}}_i \times \hat{\mathbf{P}}_a.$$
(20)

Note that the first is of the type commonly used in tight-binding calculations and similar to that employed in rtTDDFT,

while the second represents its generalization, as discussed in the previous section. Further details on the evaluation of the orbital momentum matrix elements are given in Appendix C. In particular, we should notice that the total COM commutes with the crystal field Hamiltonian and therefore it is convenient to expand it over the $\hat{H}_{\text{ie}}^0$ eigenstates; the local orbital momentum operator $\hat{\mathbf{L}}_a^0$, instead, is independent of the properties of the full system's Hamiltonian.

In Fig. 3 we evolve the electronic system under the action of the Hamiltonian (17), by approximating the spin-orbit coupling operator with Eq. (18) or with the complete spin-orbit coupling of Eq. (19). The different sets of parameters used in the calculations are provided in the figure's caption, and we assume the atoms to be fixed in their initial positions. We distinguish the evolution of the observables obtained with spin-orbit coupling (19) from the ones obtained with spin-orbit (18) by using respectively $\langle \dots \rangle$ and $\langle \dots \rangle_0$ for the expectation values.

As expected $\langle \hat{J}_z \rangle = \langle \hat{\mathcal{L}}_z \rangle + \langle \hat{S}_z \rangle$ is a constant of motion after the external electric-field pulse has vanished (see the solid blue line in the three plots on the right-hand side of Fig. 3 after $t = 10$ fs), while $\langle \hat{J}_z \rangle_0 = \langle \hat{L}_z^0 \rangle_0 + \langle \hat{S}_z \rangle_0$ is not (see dotted blue lines). Thus, the total orbital momentum is, in general, not conserved under the Hamiltonian including the approximated spin-orbit coupling interaction. The expectation value of the total orbital momentum $\langle \hat{L}_z^0 \rangle$ is also not conserved for both types of evolution (see red dotted and solid lines). The dynamics of $\langle \hat{L}_z^0 \rangle_0$ is oscillatory with the frequency that depends on the strength of the spin-orbit interaction, while the dynamics of $\langle \hat{L}_0^z \rangle$ appears to be not as strongly dependent on the spin-orbit interaction.

The plots on the left-hand side of Fig. 3 show the temporal evolution of the two observables $\langle \hat{S}_z \rangle$ and $\langle \hat{S}_z \rangle_0$. Their evolution is, not surprisingly, quite different, due to the fact that the operator $\hat{\boldsymbol{\mathcal{L}}}$ is dependent on the strength of the hopping terms, since $[\hat{H}_{\text{ie}}^0, \hat{\boldsymbol{\mathcal{L}}}] = 0$ must always be satisfied. The spin decay appears more pronounced for stronger spin-orbit interaction, although, for the same value of λ, it seems that the effect of the hopping terms should not be neglected either. In Fig. 4 we study the time evolution of a three-atom system initiated by an externally applied laser pulse and driven by two different models of spin-orbit coupling. The figure shows the evolution of the spin expectation values $\langle \hat{S}_z \rangle$ and $\langle \hat{S}_z \rangle_0$ when the spin-orbit coupling strength is fixed and the hopping terms are set to the values given in the caption. This choice of the parameters has no particular meaning from a physical point of view, and our purpose is to show how the choice may affect the orbital momentum operator $\hat{\boldsymbol{\mathcal{L}}}$ and in turn the spin-orbit coupling, while its strength λ is kept fixed. The evolution under the two spin-orbit operators is clearly different; in particular we observe that the nonapproximated one [Eq. (19)] leads to a greater loss of spin magnetization compared to the results obtained with the approximated evolution [Eq. (18)]. The effect in the case of real magnetic system is still to be investigated, but already at this level it is clear that the two spin-orbit operators may lead to different rates of spin decay thanks to the different nature of the orbital operators $\hat{\boldsymbol{\mathcal{L}}}$ and $\hat{\mathbf{L}}_0$. The fact that the COM operator describes in addition to the localized orbital properties also the orbital properties of
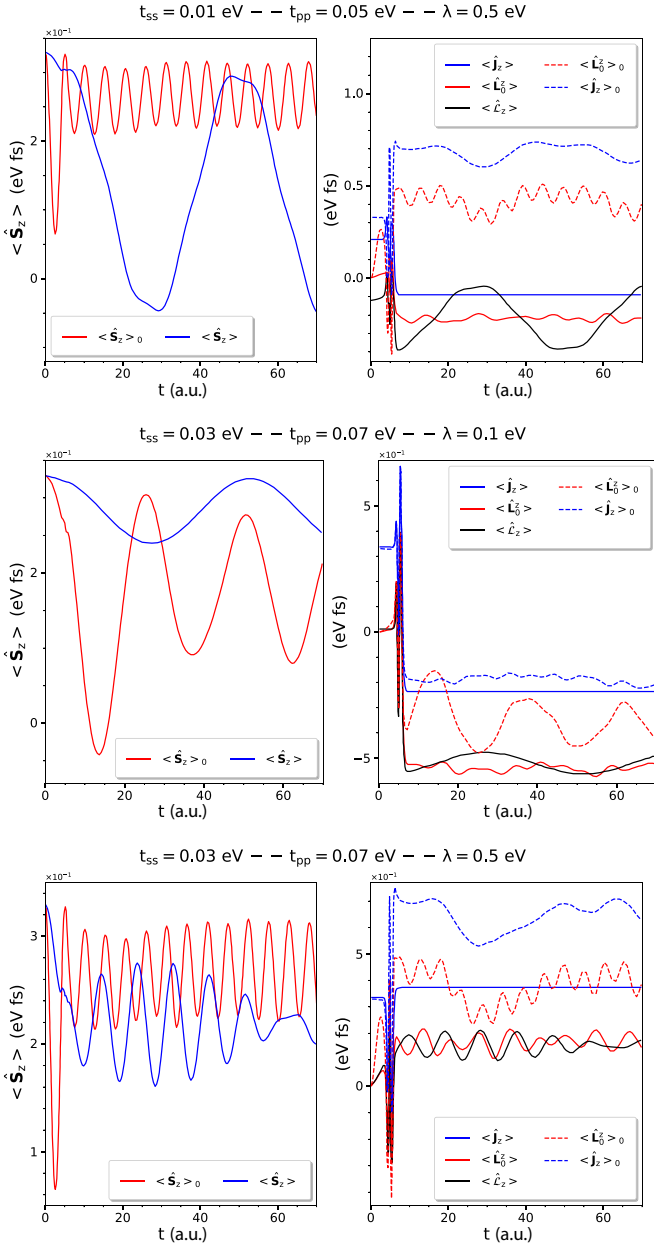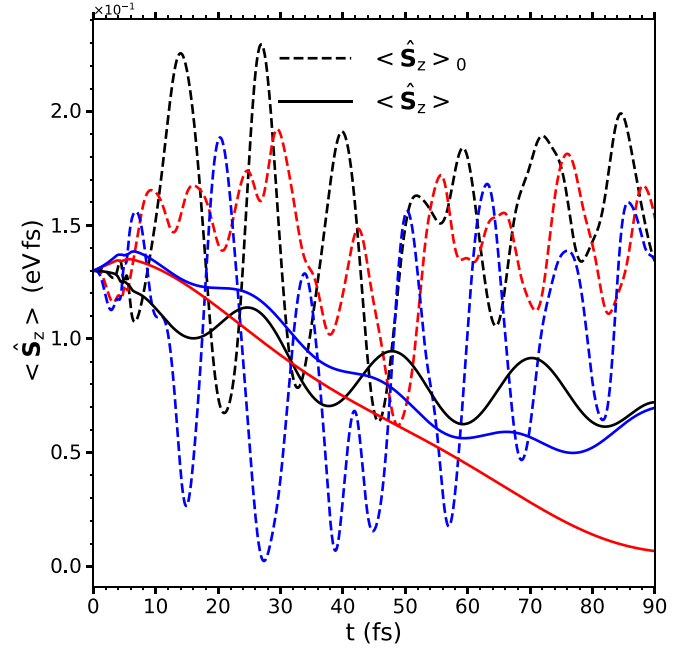
FIG. 4. Time evolution of the observables $\langle \hat{S}_z \rangle$ (solid lines) and $\langle \hat{S}_z \rangle_0$ (dashed lines) for the different models of spin-orbit coupling in the case of a three-atom system. The spin-orbit strength is fixed to a value $\lambda = 0.2$ eV, $t_{ss} = 0.03$ eV while $t_{sp} \simeq t_{pp}$ have values $\simeq 0.12$ eV (black curves), $\simeq 0.22$ eV (red curves), and $\simeq 0.32$ eV (blue curves). The external electric field is applied along one of the bond axes.

B. Coupling between electrons and molecular vibrations

In this section we briefly consider the effect of molecular vibrations on the spin dynamics. In order to account for this effect our tight-binding Hamiltonian is modified to write

$$\hat{\tilde{H}}_{\text{ie}}^{[\mathbf{R}]}(t) = \sum_{a=1}^{N_i} \sum_i \epsilon_{ai} \hat{c}_{ai}^\dagger \hat{c}_{ai} - \sum_{a<b} \sum_{i<j} \left[t_{ab}^{ij}(\mathbf{R}) \hat{c}_{bj}^\dagger \hat{c}_{ai} + \text{H.c.} \right]$$

$$- \sum_{a<b} \delta \mathbf{R}(t) \cdot \sum_{i<j} \left[\nabla t_{ab}^{ij}(\mathbf{R}) \hat{c}_{bj}^\dagger \hat{c}_{ai} + \text{H.c.} \right] + \hat{H}_{\text{SO}}^{[\mathbf{R}]}$$

$$+ \hat{H}_{\text{SO}}^{[\mathbf{R}](1)} + \hat{\mathbf{D}} \cdot \mathbf{E}(t), \qquad (21)$$

where all the terms have the usual meaning and in addition $\delta \mathbf{R}_a(t)$ indicates the atomic vibration associated to atom a, $\nabla t_{ab}^{ij}(\mathbf{R})$ represents the transition matrix elements of the gradient of the electron-ion Hamiltonian $\hat{H}_{\text{ie}}^0$, and $\hat{H}_{\text{SO}}^{[\mathbf{R}](1)}$ is an additional contribution to the spin-orbit coupling of Eq. (19) arising when the atomic vibrations carry orbital momentum. From Eq. (14) it is straightforward to show that

$$\hat{H}_{\text{SO}}^a = -\frac{\partial_r \tilde{v}_{\text{ie}}(r)}{2m_e^2 c^2 |\hat{\mathbf{r}} - \hat{\mathbf{R}}_a|} \hat{\mathbf{S}} \cdot \left[\hat{\boldsymbol{\mathcal{L}}}_a^0 + \delta \hat{\mathbf{R}}_a \times \hat{\mathbf{P}}_a \right] \qquad (22)$$

with the second term on the right-hand side corresponding to the spin-vibration contribution $\hat{H}_{\text{SO}}^{[\mathbf{R}](1)}$, while $\hat{\boldsymbol{\mathcal{L}}}_a^0 = (\mathbf{R}_a^0 - \hat{\mathbf{r}}) \times \hat{\mathbf{P}}_a$ is the orbital momentum in the absence of atomic vibrations. In Fig. 5 we analyze the effect of these additional terms to the overall spin dynamics of a magnetic cluster of 5 atoms excited by the application of an external laser pulse

FIG. 3. Time evolution of different observables for the atomic dimer excited by the application of an external laser field $E_x(t)$ slightly tilted with respect to the bond axis, with the effect of the atomic motion being neglected. In the upper plots we use a spin-orbit strength $\lambda = 0.5$ eV and hopping parameters $t_{ss} = 0.01$ eV, $t_{pp} = 0.05$ eV; we consider the expectation values $\langle \ldots \rangle$ obtained by evolving the system's Hamiltonian with spin-orbit coupling from Eq. (19) and $\langle \ldots \rangle_0$ obtained by using the Hamiltonian with approximated spin-orbit from Eq. (18). In the plots on the left-hand side we compare the expectation value of the spin, $\hat{S}_z$, for the two calculations, while in the plots on the right-hand side we compare instead the expectation values of $\hat{L}_z^0$, $\hat{J}_z$ for the two calculations with $\langle \hat{\boldsymbol{\mathcal{L}}}_z \rangle$. For the middle plots we perform the same calculations with parameters $\lambda = 0.1$ eV and $t_{ss} = 0.03$ eV, $t_{pp} = 0.07$ eV, while in the lower plots we use $\lambda = 0.5$ eV and $t_{ss} = 0.03$ eV, $t_{pp} = 0.07$ eV.

the delocalized electronic states leads to an additional contribution to the spin-orbit operator with a nontrivial influence on the dynamical evolution of the magnetic system.
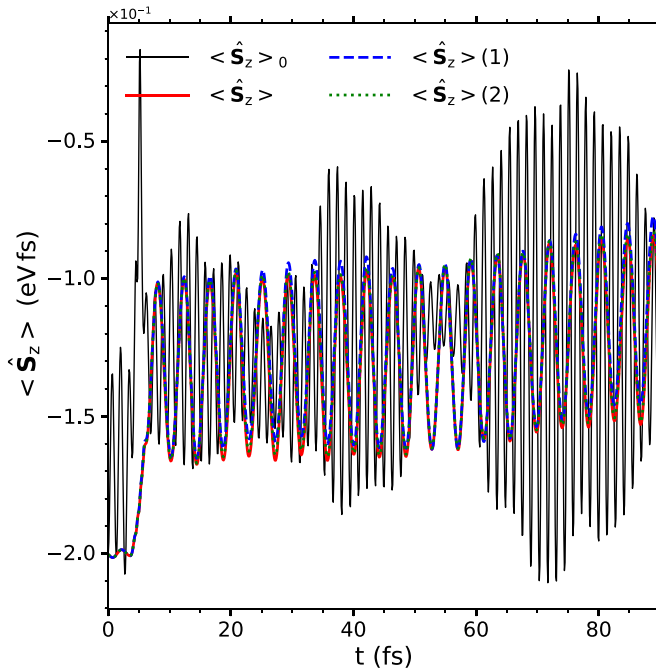
FIG. 5. Time evolution of the observables $\langle \hat{S}_z \rangle$ (solid red lines) and $\langle \hat{S}_z \rangle_0$ (solid black lines) for the different models of spin-orbit coupling and without considering molecular vibrations in the case of a five-atom system. The other two lines represent $\langle \hat{S}_z \rangle$ obtained by using two different amplitudes of atomic vibrations, namely 0.03 Å [green dotted line (2)] and 0.1 Å [blue dashed line (1)].

(the cluster has a pyramidal geometry with 4 atoms in plane and an additional atom out of plane). The vibrational orbital momentum acts also as an external field and its effect on the spin is shown in the figure for two different amplitudes of the vibrations 0.1 Å (blue dashed line) and 0.03 Å (green dotted line) and compared with the evolution in absence of vibrations for the exact (red line) and the approximated (black line) spin-orbit interaction. The effect does not seem particularly relevant at these timescales with only a noticeable change in the amplitude of the oscillations, while the evolution under the approximated spin-orbit interaction leads to huge modifications in the spin dynamics, as we have already observed.

V. CONCLUSIONS AND FUTURE WORKS

In this work we have discussed how to properly account for the conservation of the total orbital momentum in state-of-the-art *ab initio* simulations of ultrafast demagnetization processes. We have identified the main problem behind the observed breaking of the full rotational invariance to be associated with the standard implementation of the spin-orbit coupling operator. We have then explained why an approximated spin-orbit coupling operator, built as a function of the isolated atom orbital momentum, $\hat{L}^0$, may lead to difficulties in the estimation of the spin and orbital momentum temporal evolution. A proper analysis of the ultrafast demagnetization process should not be limited to the correct description of the electron-atom (phonon) channel of energy and orbital momentum dissipation, but should be based also

on a more accurate description of the spin-orbit coupling interaction. In Sec. IV we have then shown how, even for simple models, an oversimplified description of the spin-orbit coupling may affect the temporal evolution of the spin magnetization. These results are preliminary and based on simple tight-binding Hamiltonians. At this point they only aim to show the importance of these new effects. In the future, the model will be extended to describe more realistic systems (bulk materials and transition metal atomic clusters).

This new description of the ultrafast spin dynamics has some interesting consequences and it may help in shedding some light on the issue of the nonconservation of the orbital momentum observed in experiments [26,42]. Experimentally, the measure of the electronic orbital momentum is performed by means of x-ray magnetic circular dichroism (XMCD), which provides separate information on the dynamics of the spin and the electronic orbital momentum. However, it is the expectation value of $\hat{L}^0$, which is not a globally conserved quantity, to be directly accessible through these methods. In transition metals, the COM $\hat{\mathcal{L}}_a$ is expected to significantly differ from $\hat{L}_a^0$ around each atom, suggesting that the missing orbital momentum observed in experiments does not necessarily have to be instantaneously transferred to the nuclei, but it could remain hidden in the form of delocalized electronic orbital momentum for a longer time before being transferred to the lattice.

The transfer of orbital momentum to the nuclear degrees of freedom is, in fact, controlled by the electron-phonon coupling strength and it is expected to take place, in transition metals, on the slightly longer timescale of a few hundred femtoseconds (see for instance [43,44] for calculations of relaxation rates in metals such as iron and nickel and comparison with experimental data). The relaxation rate in the case of these metals has been computed and it is of the order of $\tau_E \simeq 400$ fs, approximately twice as long as the reported value of the orbital momentum relaxation time $\tau_L \simeq 200$ fs [26] even if both are related to the equilibration time of phonon and electron subsystems. The fact that $\langle \hat{L}_a^0 \rangle$ is not a measure of the total electronic orbital momentum of the system may explain why the measured rate τ_L is faster than τ_E, given that the dynamics of $\langle \hat{L}_a^0 \rangle$ is not expected to follow the temporal evolution of the lattice orbital momentum (the two quantities should not be correlated). Of course in the limit of an ensemble of isolated atoms the two approaches are completely equivalent, but this is only an idealized case, which does not correspond to any observed condition in real materials. In general, the two models are expected to differ at a rate that is inversely proportional to the degree of spin localization of the electronic system. In transition metals this effect may become rather relevant, even if a more detailed analysis is required in order to draw more definitive conclusions.
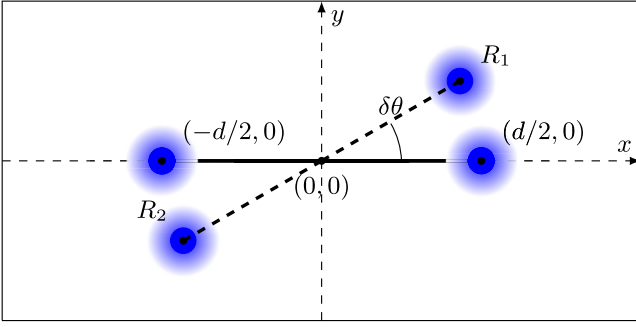
FIG. 6. Picture of the homonuclear dimer that we are using as a model system for the analysis of the orbital momentum conservation. In its initial configuration the bonding axis is along directed along x; in its successive configuration the entire dimer is rotated by an infinitesimal angle $\delta\theta$ around the out-of-plane z axis.

APPENDIX A: PROOF OF EQ. (7)

We take Eq. (6) and we sum over all the ions a on the left- and the right-hand side,

$$\frac{d}{dt}\sum_{a=1}^{N_i}\hat{\boldsymbol{\mathcal{L}}}_a = -\frac{1}{m_e}\sum_{i=1}^{N_e}\hat{\mathbf{p}}_i \times \sum_{a=1}^{N_i}\hat{\mathbf{P}}_a + \sum_{i=1}^{N_e}\hat{\mathbf{r}}_i \times \sum_{a=1}^{N_i}\boldsymbol{\nabla}_{\mathbf{R}_a}\hat{V}_{\text{ii}}$$
$$- \sum_{a=1}^{N_i}\hat{\mathbf{R}}_a \times \boldsymbol{\nabla}_{\mathbf{R}_a}\hat{V}_{\text{ii}}. \tag{A1}$$

The first term on the right-hand side is exactly zero due to the conservation of the linear momentum, $\sum_{i=1}^{N_e}\hat{\mathbf{p}}_i = -\sum_{a=1}^{N_i}\hat{\mathbf{P}}_a$. The second term is also zero. In Gaussian units we write

$$\sum_{i=1}^{N_e}\hat{\mathbf{r}}_i \times \sum_{a=1}^{N_i}\boldsymbol{\nabla}_{\mathbf{R}_a}\hat{V}_{\text{ii}} = \sum_{i=1}^{N_e}\hat{\mathbf{r}}_i \times \sum_{a=1}^{N_i}\sum_{a'\neq a}\boldsymbol{\nabla}_{\mathbf{R}_a}\frac{(Ze)^2}{|\mathbf{R}_a - \mathbf{R}_{a'}|}$$
$$= \sum_{i=1}^{N_e}\hat{\mathbf{r}}_i \times \sum_{a=1}^{N_i}\sum_{a\neq a'}\left[-\frac{(Ze)^2\hat{\mathbf{R}}_a}{|\mathbf{R}_a - \mathbf{R}_{a'}|} + \frac{(Ze)^2\hat{\mathbf{R}}_{a'}}{|\mathbf{R}_a - \mathbf{R}_{a'}|}\right]$$
$$= 0. \tag{A2}$$

Analogously for the third term we have

$$\sum_{a=1}^{N_i}\hat{\mathbf{R}}_a \times \boldsymbol{\nabla}_{\mathbf{R}_a}\hat{V}_{\text{ii}} = \sum_{a=1}^{N_i}\sum_{a'\neq a}(Ze)^2\frac{\hat{\mathbf{R}}_a \times \hat{\mathbf{R}}_{a'}}{|\mathbf{R}_a - \mathbf{R}_{a'}|^3}$$
$$= \frac{(Ze)^2}{2}\sum_{a=1}^{N_i}\sum_{a'\neq a}\left[\frac{\hat{\mathbf{R}}_a \times \hat{\mathbf{R}}_{a'}}{|\mathbf{R}_a - \mathbf{R}_{a'}|^3} - \frac{\hat{\mathbf{R}}_a \times \hat{\mathbf{R}}_{a'}}{|\mathbf{R}_a - \mathbf{R}_{a'}|^3}\right]$$
$$= 0, \tag{A3}$$

which finally proves Eq. (7), namely, that the operator $\sum_{a=1}^{N_i}\hat{\boldsymbol{\mathcal{L}}}_a$ is a constant of motion for the system's Hamiltonian $\hat{H}$.

APPENDIX B: PROOF OF INEQUALITY (8)

Here we explicitly verify the inequality (8) for the electronic orbital momentum. The simplest possible case we may

consider here is that of a homonuclear diatomic molecule (see Fig. 6; the nature of the atoms is not relevant), with wave functions expanded over a minimal basis of s, p_x, p_y, and p_z orbitals with no spin polarization. Here we do not want to describe a realistic situation, just prove conceptually that the orbital momentum of the atomic plus electronic subsystem cannot be conserved in general if we employ the operators $\hat{\mathbf{L}}_a^0$ to describe the electronic orbital momentum. According to Fig. 6 we assume that the dimer is uniformly rotating around the z axis (out of plane) by an infinitesimal angle $\delta\theta$, the length of the bond is d, the Hamiltonian and orbital momentum operators are expanded over the atomic basis set $\{|1;s\rangle, |1;p_{-1}\rangle, |1;p_0\rangle, |1;p_1\rangle, |2;s\rangle, |2;p_{-1}\rangle, |2;p_0\rangle, |2;p_1\rangle\}$, and in the new rotated configuration we can write

$$\hat{L}_z^0 = \left(\begin{array}{c|c}\mathbb{L}_{1,z}^0 & \mathbf{0} \\ \hline \mathbf{0} & \mathbb{L}_{2,z}^0\end{array}\right)$$

$$= \begin{bmatrix}0 & 0 & 0 & 0 & 0 & 0 & 0 & 0 \\ 0 & -1 & 0 & 0 & 0 & 0 & 0 & 0 \\ 0 & 0 & 0 & 0 & 0 & 0 & 0 & 0 \\ 0 & 0 & 0 & 1 & 0 & 0 & 0 & 0 \\ 0 & 0 & 0 & 0 & 0 & 0 & 0 & 0 \\ 0 & 0 & 0 & 0 & 0 & -1 & 0 & 0 \\ 0 & 0 & 0 & 0 & 0 & 0 & 0 & 0 \\ 0 & 0 & 0 & 0 & 0 & 0 & 0 & 1\end{bmatrix}, \tag{B1}$$

which corresponds to the total electronic orbital momentum operator, obtained as a direct sum of the orbital momentum operators corresponding to the two isolated atomic sites, $\hat{\mathbf{L}}^0 = \hat{\mathbf{L}}_1^0 \oplus \hat{\mathbf{L}}_2^0$. The Hamiltonian $\hat{H}_{\text{ie}}$ of the system, in turn, depends on 4 free parameters, the on-site orbital energies ϵ_s, ϵ_p (we assume degeneracy of the p orbitals for simplicity), and the hopping coefficients depend on a set of primitive integrals t_{ss}, t_{sp}, t_{pp}^σ, and t_{pp}^π that here are left arbitrary but in general are a function of the distance between the two atoms of the dimer molecule. These integrals $t_{ij}^{nlm_a;n'l'm_a'}$ are diagonal in the angular momentum projection m_a along the bond axis and do not depend on its sign [45], $t_{ij}^{nlm_a;n'l'm_a'} = t_{ij}^{nl|m_a|;n'l'|m_a|}\delta_{m_a,m_a'}$. These can be written through the following general expression:

$$t_{ij}^{nlm_a,n'l'm_a} = \int_V d^3\mathbf{r}\,\psi_{nlm_a}^*(\mathbf{r} - \mathbf{R}_i)h_{ij}(\mathbf{r})\psi_{n'l'm_a}(\mathbf{r} - \mathbf{R}_j),$$
$$\tag{B2}$$

where ψ_{nlm_a} is an atomic wave function and $h_{ij}(\mathbf{r}) = -\hbar^2\nabla^2/2m_e + v_{\text{ie}}(\mathbf{r} - \mathbf{R}_i) + v_{\text{ie}}(\mathbf{r} - \mathbf{R}_j)$; the free hopping parameters are given by the following two-center integrals:

$$t_{ss} = \langle n=2, l=0, m_a=0|\hat{h}_{12}|n=2, l'=0, m_a=0\rangle,$$
$$t_{sp} = \langle n=2, l=0, m_a=0|\hat{h}_{12}|n=2, l'=1, m_a=0\rangle,$$
$$t_{pp}^\sigma = \langle n=2, l=1, m_a=0|\hat{h}_{12}|n=2, l'=1, m_a=0\rangle,$$
$$t_{pp}^\pi = \langle n=2, l=1, m_a=1|\hat{h}_{12}|n=2, l'=1, m_a=1\rangle.$$

In addition we also have the exact relation $t_{ij}^{nlm_a,n'l'm_a} = (-1)^{l+l'}t_{ji}^{nlm_a,n'l'm_a}$ that leads to the final expression for the dimer's Hamiltonian,

$$
\hat{H}_{\mathrm{ie}} =
\begin{bmatrix}
\epsilon_s & 0 & 0 & 0 & t_{ss} & \frac{\lambda_- t_{sp}}{\sqrt{2}} & t_{sp}\lambda_z & -\frac{\lambda_+ t_{sp}}{\sqrt{2}} \\[4pt]
0 & \epsilon_p & 0 & 0 & -\frac{\lambda_- t_{sp}}{\sqrt{2}} & \frac{t_{pp}^\sigma+t_{pp}^\pi-\lambda_z^2\Delta t_{pp}}{2} & \frac{\lambda_z\lambda_-\Delta t_{pp}}{\sqrt{2}} & -\frac{\lambda_-^2\Delta t_{pp}}{2} \\[4pt]
0 & 0 & \epsilon_p & 0 & -t_{sp}\lambda_z & \frac{\lambda_z\lambda_-\Delta t_{pp}}{\sqrt{2}} & \lambda_z^2\Delta t_{pp}+t_{pp}^\pi & -\frac{\lambda_z\lambda_+\Delta t_{pp}}{\sqrt{2}} \\[4pt]
0 & 0 & 0 & \epsilon_p & \frac{\lambda_+ t_{sp}}{\sqrt{2}} & -\frac{\lambda_-^2\Delta t_{pp}}{2} & -\frac{\lambda_z\lambda_+\Delta t_{pp}}{\sqrt{2}} & \frac{t_{pp}^\sigma+t_{pp}^\pi-\lambda_z^2\Delta t_{pp}}{2} \\[4pt]
t_{ss} & -\frac{\lambda_+}{\sqrt{2}}t_{sp} & -t_{sp}\lambda_z & \frac{\lambda_-}{\sqrt{2}}t_{sp} & \epsilon_s & 0 & 0 & 0 \\[4pt]
\frac{\lambda_+}{\sqrt{2}}t_{sp} & \frac{t_{pp}^\sigma+t_{pp}^\pi-\lambda_z^2\Delta t_{pp}}{2} & \frac{\lambda_z\lambda_+}{\sqrt{2}}\Delta t_{pp} & -\frac{\lambda_-^2}{2}\Delta t_{pp} & 0 & \epsilon_p & 0 & 0 \\[4pt]
t_{sp}\lambda_z & \frac{\lambda_z\lambda_+}{\sqrt{2}}\Delta t_{pp} & \lambda_z^2\Delta t_{pp}+t_{pp}^\pi & -\frac{\lambda_z\lambda_-}{\sqrt{2}}\Delta t_{pp} & 0 & 0 & \epsilon_p & 0 \\[4pt]
-\frac{\lambda_-}{\sqrt{2}}t_{sp} & -\frac{\lambda_+^2}{2}\Delta t_{pp} & -\frac{\lambda_z\lambda_-}{\sqrt{2}}\Delta t_{pp} & \frac{t_{pp}^\sigma+t_{pp}^\pi-\lambda_z^2\Delta t_{pp}}{2} & 0 & 0 & 0 & \epsilon_p
\end{bmatrix},
$$

where we have used $\Delta t_{pp} = t_{pp}^\sigma - t_{pp}^\pi$; the dimer bond length is $d = |\mathbf{R}_1 - \mathbf{R}_2|$ with $\lambda_{x,y,z} = (\mathbf{R}_1 - \mathbf{R}_2)_{x,y,z}/|\mathbf{R}_1 - \mathbf{R}_2|$ and $\lambda_\pm = \lambda_x \pm i\lambda_y$.

In the rotated configuration we have $(\mathbf{R}_1 - \mathbf{R}_2)_x = d\cos\delta\theta$, $(\mathbf{R}_1 - \mathbf{R}_2)_y = d\sin\delta\theta$, and we can substitute in the Hamiltonian

$$\lambda_\pm = 1 - \frac{\delta\theta^2}{2} \pm i\delta\theta, \tag{B3}$$

$$\lambda_z = 0. \tag{B4}$$

The new atomic coordinates according to Fig. 6 are given by $\mathbf{R}_1 = \frac{d}{2}(\cos\delta\theta, \sin\delta\theta, 0)$, $\mathbf{R}_2 = -\frac{d}{2}(\cos\delta\theta, \sin\delta\theta, 0)$. The time derivative of the orbital momentum of the two atoms is given by

$$\dot{\mathbf{L}}_1 = -\mathbf{R}_1 \times \nabla_{\mathbf{R}_1}\langle\delta\hat{H}_{\mathrm{ie}}\rangle = -\mathbf{R}_1 \times \nabla_{\mathbf{R}_1}\delta\theta \cdot \partial_{\delta\theta}\langle\delta\hat{H}_{\mathrm{ie}}\rangle,$$
$$\dot{\mathbf{L}}_2 = -\mathbf{R}_2 \times \nabla_{\mathbf{R}_2}\langle\delta\hat{H}_{\mathrm{ie}}\rangle = -\mathbf{R}_2 \times \nabla_{\mathbf{R}_2}\delta\theta \cdot \partial_{\delta\theta}\langle\delta\hat{H}_{\mathrm{ie}}\rangle,$$

and the total orbital momentum time derivative becomes

$$\dot{\mathbf{L}}^{\mathrm{atom}} = \dot{\mathbf{L}}_1 + \dot{\mathbf{L}}_2 = -\partial_{\delta\theta}\langle\hat{H}_{\mathrm{ie}}\rangle \cdot (\mathbf{R}_1 - \mathbf{R}_2) \times \nabla_{\mathbf{R}_1}\delta\theta$$
$$= -4\hat{\mathbf{e}}_z \cdot \partial_{\delta\theta}\langle\hat{H}_{\mathrm{ie}}\rangle. \tag{B5}$$

In order to simplify the calculation we proceed by assuming that we have a single electron in a state given by the superposition of $|1; s\rangle$ around atom 1 and $|2; p_{-1}\rangle$ around atom 2; $|\Psi\rangle = [1, 0, 0, 0, 0, 1, 0, 0]/\sqrt{2}$ in the same basis of the Hamiltonian. By explicitly computing Eq. (B5) we obtain at first order in $\delta\theta$

$$\partial_{\delta\theta}\langle\hat{H}_{\mathrm{ie}}\rangle = -\frac{t_{sp}}{\sqrt{2}}\delta\theta,$$
$$\dot{\mathbf{L}}^{\mathrm{atom}} = 2\sqrt{2} \cdot \hat{\mathbf{e}}_z t_{sp}\delta\theta. \tag{B6}$$

The time derivative of the expectation value of the electronic orbital momentum is given by ($\hbar$ is set to 1)

$$\frac{d}{dt}\langle\hat{L}_z^0\rangle = i\langle[\hat{H}_{\mathrm{ie}}, \hat{L}_z^0]\rangle, \tag{B7}$$

which explicitly computed by using the wave function $|\Psi\rangle$ previously defined gives

$$\frac{d}{dt}\langle\hat{L}_z^0\rangle = -\frac{t_{sp}}{\sqrt{2}}\delta\theta. \tag{B8}$$

The time derivative of the total orbital momentum $\dot{\mathbf{L}}^{\mathrm{atom}} + \frac{d}{dt}\langle\hat{L}_z^0\rangle$ along the z axis is

$$\dot{L}_z^{\mathrm{atom}} + \frac{d}{dt}\langle\hat{L}_z^0\rangle = \frac{3}{\sqrt{2}}t_{sp}\delta\theta, \tag{B9}$$

which proves Eq. (7) in the main text.

APPENDIX C: COM OPERATOR MATRIX ELEMENTS

By assuming that the atoms behave as classical particles, while the electrons, as mentioned in the main text, are treated as effective noninteracting particles, the operator $\sum_a \hat{\mathcal{L}}_a$ may be written as ($\sum_a \hat{\mathbf{P}}_a = -\hat{\mathbf{p}}$)

$$\sum_{a=1}^{N_i} \hat{\mathcal{L}}_a = \sum_{a=1}^{N_i} \mathbf{R}_a \times \mathbf{P}_a + \hat{\mathbf{r}} \times \hat{\mathbf{p}}, \tag{C1}$$

corresponding to the expression of the system total angular momentum. The atomic part is just a number, and in all the cases considered is set to zero, so we focus on the electronic part that can be expressed in a more suitable form,

$$\hat{\mathbf{L}}^{\mathrm{e}} = \frac{im_{\mathrm{e}}}{\hbar}\hat{\mathbf{r}} \times [\hat{H}_{\mathrm{ie}}^0, \hat{\mathbf{r}}]. \tag{C2}$$

The matrix elements between two atomic basis centered states on the atomic sites $\mathbf{R}_1$ and $\mathbf{R}_2$ are [by labeling $\alpha = (n, l, m)$ and $\beta = (n', l', m')$] after some manipulation

$$
\begin{aligned}
&\langle\alpha; \mathbf{R}_1|\hat{\mathbf{L}}^{\mathrm{e}}|\beta; \mathbf{R}_2\rangle \\
&= \frac{im_{\mathrm{e}}}{\hbar}\mathbf{R}_1 \times \mathbf{R}_2\langle\alpha; \mathbf{R}_1|\hat{H}_{\mathrm{ie}}^0|\beta; \mathbf{R}_2\rangle \\
&\quad + \frac{im_{\mathrm{e}}}{\hbar}\sum_\gamma \mathbf{D}_{\alpha\gamma}(\mathbf{R}_1) \times (\mathbf{R}_2 - \mathbf{R}_1)\langle\gamma; \mathbf{R}_1|\hat{H}_{\mathrm{ie}}^0|\beta; \mathbf{R}_2\rangle \\
&\quad + \frac{im_{\mathrm{e}}}{\hbar}\sum_\eta \mathbf{R}_1 \times \big[\langle\alpha; \mathbf{R}_1|\hat{H}_{\mathrm{ie}}^0|\eta; \mathbf{R}_2\rangle\mathbf{D}_{\eta\beta}(\mathbf{R}_2) \\
&\quad - \mathbf{D}_{\alpha\eta}(\mathbf{R}_1)\langle\eta; \mathbf{R}_1|\hat{H}_{\mathrm{ie}}^0|\beta; \mathbf{R}_2\rangle\big] + \frac{im_{\mathrm{e}}}{\hbar}\sum_{\gamma,\eta}\mathbf{D}_{\alpha\gamma}(\mathbf{R}_1) \\
&\quad \times \big[\langle\gamma; \mathbf{R}_1|\hat{H}_{\mathrm{ie}}^0|\eta; \mathbf{R}_2\rangle\mathbf{D}_{\eta\beta}(\mathbf{R}_2) \\
&\quad - \mathbf{D}_{\alpha\eta}(\mathbf{R}_1)\langle\eta; \mathbf{R}_1|\hat{H}_{\mathrm{ie}}^0|\beta; \mathbf{R}_2\rangle\big], \tag{C3}
\end{aligned}
$$

where we have used $\langle\alpha;\mathbf{R}_1|\hat{\mathbf{r}}|\gamma;\mathbf{R}_2\rangle = [\mathbf{R}_1\delta_{\alpha,\gamma} + \mathbf{D}_{\alpha\gamma}(\mathbf{R}_1)]\delta(\mathbf{R}_1 - \mathbf{R}_2)$.

In the limit of a system of isolated atoms the operator $\hat{\mathbf{L}}^e$ must reduce to the sum of the isolated atoms' orbital momenta, $\sum_a \hat{\mathbf{L}}_a^0 = \hat{\mathbf{L}}^0$. In this limit the Hamiltonian matrix elements are $\langle\alpha;\mathbf{R}_1|\hat{H}_{ie}^0|\beta;\mathbf{R}_2\rangle = \epsilon_{\alpha,1}\delta_{\alpha,\beta}\delta(\mathbf{R}_1 - \mathbf{R}_2)$ and we can rewrite the orbital momentum matrix elements as follows:

$$\mathbf{L}_{\alpha\beta}^0(\mathbf{R}) = \frac{im_e}{\hbar}\mathbf{R} \times \mathbf{D}_{\alpha\beta}(\mathbf{R})(\epsilon_\alpha - \epsilon_\beta)$$
$$+ \frac{im_e}{\hbar}\sum_\gamma \epsilon_\gamma \mathbf{D}_{\alpha\gamma}(\mathbf{R}) \times \mathbf{D}_{\gamma\beta}(\mathbf{R})$$
$$- \frac{im_e}{\hbar}\sum_\gamma \epsilon_\beta \mathbf{D}_{\alpha\gamma}(\mathbf{R}) \times \mathbf{D}_{\alpha\beta}(\mathbf{R}). \tag{C4}$$

We can then set

$$\langle\alpha;\mathbf{R}_1|\hat{\mathbf{L}}^e|\beta;\mathbf{R}_2\rangle = \begin{cases} \mathbf{L}_{\alpha\beta}^0(\mathbf{R}_1), & \mathbf{R}_1 = \mathbf{R}_2, \\ \text{Eq. (C3)}, & \mathbf{R}_1 \neq \mathbf{R}_2, \end{cases}$$

in such a way to recover the correct limit for isolated atoms. The temporal evolution of the electronic orbital momentum is then written as (in the absence of spin-orbit coupling)

$$\frac{d}{dt}\hat{\mathbf{L}}^e = \sum_{a=1}^{N_i} \mathbf{R}_a \times \nabla_{\mathbf{R}_a}\hat{H}_{ie}^0. \tag{C5}$$

With no atomic motion, as are all the cases considered here, the right-hand side of the previous expression is zero and $\hat{\mathbf{L}}^e$ does not need to be updated in time. In order to preserve the commutation rules, $\hat{\mathcal{L}} = \hat{\mathbf{L}}^e$ is expanded over the eigenvector basis set of $\hat{H}_{ie}^0$, $\{|\lambda_m\rangle\}$,

$$\hat{\mathbf{L}}^e = \sum_n |\lambda_n\rangle\langle\lambda_n|\hat{\mathbf{L}}^e|\lambda_n\rangle\langle\lambda_n|. \tag{C6}$$

$\hat{\mathbf{L}}_a^e$ is then obtained by projecting over the local atom basis set $\hat{\mathbf{L}}_a^e = \hat{\Pi}_a^\dagger \hat{\mathbf{L}}^e \hat{\Pi}_a$. In the presence of spin-orbit coupling the considerations are the same and the procedure must be repeated with the only difference that now the conserved quantity is $\hat{\mathbf{J}} = \hat{\mathcal{L}} + \hat{\mathbf{S}}$ and it should be projected over the eigenstates of the crystal field Hamiltonian with spin-orbit interaction. We would like to conclude by mentioning that in the presence of atomic motion, the phonons should be also evolved in time and the formalism must be revisited with the COM operator now defined over a basis set of both phononic and electronic degrees of freedom. However, during the first few femtoseconds of dynamics we expect the atomic effects to be very small and negligible given that the electronic effects are dominant.

[1] E. Beaurepaire, J.-C. Merle, A. Daunois, and J.-Y. Bigot, Ultrafast Spin Dynamics in Ferromagnetic Nickel, Phys. Rev. Lett. **76**, 4250 (1996).

[2] J.-Y. Bigot, L. Guidoni, E. Beaurepaire, and P. N. Saeta, Femtosecond Spectrotemporal Magneto-optics, Phys. Rev. Lett. **93**, 077401 (2004).

[3] J. Hohlfeld, E. Matthias, R. Knorren, and K. H. Bennemann, Nonequilibrium Magnetization Dynamics of Nickel, Phys. Rev. Lett. **78**, 4861 (1997).

[4] J. Güdde, U. Conrad, V. Jähnke, J. Hohlfeld, and E. Matthias, Magnetization dynamics of Ni and Co films on Cu(001) and of bulk nickel surfaces, Phys. Rev. B **59**, R6608(R) (1999).

[5] A. Scholl, L. Baumgarten, R. Jacquemin, and W. Eberhardt, Ultrafast Spin Dynamics of Ferromagnetic Thin Films Observed by fs Spin-Resolved Two-Photon Photoemission, Phys. Rev. Lett. **79**, 5146 (1997).

[6] G. Ju, A. V. Nurmikko, R. F. C. Farrow, R. F. Marks, M. J. Carey, and B. A. Gurney, Ultrafast Time Resolved Photoinduced Magnetization Rotation in a Ferromagnetic/Antiferromagnetic Exchange Coupled System, Phys. Rev. Lett. **82**, 3705 (1999).

[7] B. Koopmans, M. van Kampen, J. T. Kohlhepp, and W. J. M. de Jonge, Ultrafast Magneto-Optics in Nickel: Magnetism or Optics?, Phys. Rev. Lett. **85**, 844 (2000).

[8] T. Ogasawara, K. Ohgushi, Y. Tomioka, K. S. Takahashi, H. Okamoto, M. Kawasaki, and Y. Tokura, General Features of Photoinduced Spin Dynamics in Ferromagnetic and Ferrimagnetic Compounds, Phys. Rev. Lett. **94**, 087202 (2005).

[9] A. V. Kimel, A. Kirilyuk, A. Tsvetkov, R. V. Pisarev, and T. Rasing, Laser-induced ultrafast spin reorientation in the antiferromagnet TmFeO$_3$, Nature (London) **429**, 850 (2004).

[10] M. Vomir, L. H. F. Andrade, L. Guidoni, E. Beaurepaire, and J.-Y. Bigot, Real Space Trajectory of the Ultrafast Magnetization Dynamics in Ferromagnetic Metals, Phys. Rev. Lett. **94**, 237601 (2005).

[11] G. Ju, J. Hohlfeld, B. Bergman, R. J. M. van de Veerdonk, O. N. Mryasov, J. Y. Kim, X. Wu, D. Weller, and B. Koopmans, Ultrafast Generation of Ferromagnetic Order via a Laser-Induced Phase Transformation in FeRh Thin Films, Phys. Rev. Lett. **93**, 197403 (2004).

[12] J. U. Thiele, M. Buess, and C. H. Back, Spin dynamics of the antiferromagnetic-to-ferromagnetic phase transition in FeRh on a sub-picosecond time scale, Appl. Phys. Lett. **85**, 2857 (2004).

[13] A. V. Kimel, A. Kirilyuk, P. A. Usachev, R. V. Pisarev, A. M. Balbashov, and T. Rasing, Ultrafast non-thermal control of magnetization by instantaneous photomagnetic pulses, Nature (London) **435**, 655 (2005).

[14] C. D. Stanciu, F. Hansteen, A. V. Kimel, A. Kirilyuk, A. Tsukamoto, A. Itoh, and T. Rasing, All-Optical Magnetic Recording with Circularly Polarized Light, Phys. Rev. Lett. **99**, 047601 (2007).

[15] J. Berezovsky, M. H. Mikkelsen, N. G. Stoltz, L. A. Coldren, and D. D. Awschalom, Picosecond coherent optical manipulation of a single electron spin in a quantum dot, Science **320**, 349 (2008).

[16] A. V. Kimel, A. Kirilyuk, and T. Rasing, Femtosecond optomagnetism: Ultrafast laser manipulation of magnetic materials, Laser Photon. Rev. **1**, 275 (2007).

[17] A. Kirilyuk, A. V. Kimel, and T. Rasing, Ultrafast optical manipulation of magnetic order, Rev. Mod. Phys. **82**, 2731 (2010).

[18] M. Fähnle and C. Illg, Electron theory of fast and ultrafast dissipative magnetization dynamics, J. Phys.: Condens. Matter **23**, 493201 (2011).

[19] Y. Hinschberger and P.-A. Hervieux, Foldy-Wouthuysen transformation applied to the interaction of an electron with ultrafast electromagnetic fields, Phys. Lett. A **376**, 813 (2012).

[20] H. Vonesch and J. Y. Bigot, Ultrafast spin-photon interaction investigated with coherent magneto-optics, Phys. Rev. B **85**, 180407(R) (2012).

[21] E. Carpene, E. Mancini, C. Dallera, M. Brenna, E. Puppin, and S. De Silvestri, Dynamics of electron-magnon interaction and ultrafast demagnetization in thin iron films, Phys. Rev. B **78**, 174422 (2008).

[22] M. Krauss, T. Roth, S. Alebrand, D. Steil, M. Cinchetti, M. Aeschlimann, and H. C. Schneider, Ultrafast demagnetization of ferromagnetic transition metals: The role of the Coulomb interaction, Phys. Rev. B **80**, 180407(R) (2009).

[23] K. Carva, M. Battiato, and P. M. Oppeneer, *Ab Initio* Investigation of the Elliott-Yafet Electron-Phonon Mechanism in Laser-Induced Ultrafast Demagnetization, Phys. Rev. Lett. **107**, 207201 (2011).

[24] D. A. Garanin and E. M. Chudnovsky, Angular momentum in spin-phonon processes, Phys. Rev. B **92**, 024421 (2015).

[25] M. Battiato, K. Carva, and P. M. Oppeneer, Theory of laser-induced ultrafast superdiffusive spin transport in layered heterostructures, Phys. Rev. B **86**, 024404 (2012).

[26] M. Hennecke, I. Radu, R. Abrudan, T. Kachel, K. Holldack, R. Mitzner, A. Tsukamoto, and S. Eisebitt, Angular Momentum Flow during Ultrafast Demagnetization of a Ferrimagnet, Phys. Rev. Lett. **122**, 157202 (2019).

[27] D. Steiauf, C. Illg, and M. Fähnle, Demagnetization on the fs time-scale by the Elliott-Yafet mechanism, J. Phys.: Conf. Ser. **200**, 042024 (2010).

[28] M. Fähnle, T. Tsatsoulis, C. Illg, M. Haag, B. Y. Müller, and L. Zhang, Ultrafast demagnetization after femtosecond laser pulses: Transfer of angular momentum from the electronic system to magnetoelastic spin-phonon modes, J. Supercond. Novel Magn. **30**, 1381 (2017).

[29] M. Fähnle, M. Haag, and C. Illg, Is the angular momentum of a ferromagnetic sample after exposure to a fs laser pulse conserved?, J. Magn. Magn. Mater. **347**, 45 (2013).

[30] K. Krieger, J. K. Dewhurst, P. Elliott, S. Sharma, and E. K. U. Gross, Laser-induced demagnetization at ultrashort time scales: Predictions of TDDFT, J. Chem. Theory Comput. **11**, 4870 (2015).

[31] M. Stamenova, J. Simoni, and S. Sanvito, Role of spin-orbit interaction in the ultrafast demagnetization of small iron clusters, Phys. Rev. B **94**, 014423 (2016).

[32] W. Töws and G. M. Pastor, Many-Body Theory of Ultrafast Demagnetization and Angular Momentum Transfer in Ferromagnetic Transition Metals, Phys. Rev. Lett. **115**, 217204 (2015).

[33] D. Chaudhuri, G. Lefkidis, and W. Hübner, All-spin-based ultrafast nanologic elements with a Ni_4 cluster, Phys. Rev. B **96**, 184413 (2017).

[34] E. K. U. Gross and W. Kohn, Time-dependent density-functional-theory, Adv. Quantum Chem. **21**, 255 (1990).

[35] E. Runge and E. K. U. Gross, Density-Functional Theory for Time-Dependent Systems, Phys. Rev. Lett. **52**, 997 (1984).

[36] $\hat{\mathbf{L}}_{\text{electrons}}^{\text{KS}}$ is the orbital momentum of the Kohn-Sham system and it should always be distinguished from the true many-body electronic orbital momentum, $\mathbf{L}_{\text{electrons}}$. However, in order to simplify our analysis, we will assume throughout the paper that two quantities are equal to a good degree of approximation. This assumption, in fact, will not play any role in the coming considerations.

[37] M. A. L. Marques, A. Castro, G. F. Bertsch, and A. Rubio, octopus: A first-principles tool for excited electron-ion dynamics, Comput. Phys. Commun. **151**, 60 (2003).

[38] D. R. Hamann, M. Schlüter, and C. Chiang, Norm-Conserving Pseudopotentials, Phys. Rev. Lett. **43**, 1494 (1979).

[39] L. Kleinman, Relativistic norm-conserving pseudopotential, Phys. Rev. B **21**, 2630 (1980).

[40] M. J. T. Oliveira and F. Nogueira, Generating relativistic pseudo-potentials with explicit incorporation of semi-core states using APE, the atomic pseudo-potentials engine, Comput. Phys. Commun. **178**, 524 (2008).

[41] X. Andrade, A. Castro, D. Zueco, J. L. Alonso, P. Echenique, F. Falceto, and A. Rubio, Modified Ehrenfest formalism for efficient large-scale *ab initio* molecular dynamics, J. Chem. Theory Comput. **5**, 728 (2009).

[42] C. Dornes, Y. Acremann, M. Savoini, M. Kubli, M. J. Neugebauer, E. Abreu, L. Huber, G. Lantz, C. A. F. Vaz, H. Lemke, E. M. Bothschafter, M. Porer, V. Esposito, L. Rettig, M. Buzzi, A. Alberca, Y. W. Windsor, P. Beaud, U. Staub, D. Zhu, S. Song, S. L. Johnson *et al.*, The ultrafast Einstein–de Haas effect, Nature (London) **565**, 209 (2019).

[43] Z. Lin, L. V. Zhigilei, and V. Celli, Electron-phonon coupling and electron heat capacity of metals under conditions of strong electron-phonon nonequilibrium, Phys. Rev. B **77**, 075133 (2008).

[44] J. Simoni and J. Daligault, First-Principles Determination of Electron-Ion Couplings in the Warm Dense Matter Regime, Phys. Rev. Lett. **122**, 205001 (2019).

[45] P. Koskinen and V. Mäkinen, Density-functional tight-binding for beginners, Comput. Mater. Sci. **47**, 237 (2009).